Testing the Tomographic Fermi Liquid Hypothesis with High-Order Cyclotron Resonance

Ilia Moiseenko,[1] Erwin Mönch,[2] Kirill Kapralov,[1] Denis Bandurin,[3,†] Sergey Ganichev,[2] and Dmitry Svintsov[1,*]
[1]Laboratory of 2d Materials for Optoelectonics, Moscow Institute of Physics and Technology, Dolgoprudny 141700, Russia
[2]Terahertz Center, University of Regensburg, 93040 Regensburg, Germany
[3]Department of Materials Science and Engineering, National University of Singapore, Singapore 117575

(Received 2 May 2024; revised 28 February 2025; accepted 12 May 2025; published 5 June 2025)

The tomographic Fermi liquid (TFL) hypothesis posits starkly different relaxation times for odd and even angular harmonics of electron distribution function in two-dimensional systems, but its experimental verification remains elusive. Traditional electrical transport struggles to discern these lifetimes, as resistivity is largely unaffected by electron scattering. Here, we demonstrate that high-order cyclotron resonance (CR) offers a direct probe: The linewidth of the mth CR peak directly reflects the relaxation rate $\gamma_m = 1/\tau_m$ of the corresponding angular harmonic. Combining theory and terahertz photoconductivity measurements in graphene, we show that the third-order CR exhibits a narrower linewidth than the second-order CR, yielding $\tau_3 > \tau_2$. This hierarchy defies conventional impurity or phonon scattering models, instead aligning with TFL predictions where odd harmonics evade relaxation via head-on collisions. Our results provide definitive evidence for the TFL regime and establish high-order CR as a powerful tool to unravel hydrodynamic transport in quantum materials.

DOI: 10.1103/zq1g-8d4s

The concept of hydrodynamics has recently evolved beyond traditional fluid dynamics, extending its reach to the behavior of electrons in solids, particularly in low-dimensional systems such as graphene [1] and its derivatives, GaAs-based heterostructures [2], and WTe_2 [3], to name a few (see Ref. [4] for review). Since hydrodynamics provides a natural framework for exploring the behavior of strongly interacting many-body systems, experiments on model platforms supporting hydrodynamic flow can offer insights into more complex systems, such as quark-gluon plasma [5], strange metals [6], and cold atoms [7,8], substantiating interest in the field.

Electron hydrodynamics appears in interacting electron systems with momentum-conserving scattering among charge carriers dominating over other scattering processes [9]. Recent theoretical studies [10] have identified a new hydrodynamiclike transport regime in two dimensions, where electron distribution in phase space rapidly diffuses along the velocity direction, and this direction slowly rotates [11]. Such motion, reminiscent of scanning procedure in tomographs, led to the notion of "tomographic transport." Emergence of tomographic transport traces down to dramatically different relaxation times of the odd and even angular harmonics of the distribution function [12–14]. The difference stems from kinematic constraints for two-particle collisions, which are either low-angle or head-on [Figs. 1(a) and 1(b)]. Low-angle collisions always make a minor effect on momentum redistribution, while head-on collisions require two electrons at the opposite ends of Fermi surface. The momentum-odd distributions, conversely, have an electron and a hole at opposite ends [Fig. 1(b)] and are, thus, immune to the head-on collisions.

If observed, the tomographic transport would challenge the conventional concepts of hydrodynamics and Fermi liquid (FL) used to describe many-body systems. Historically, deviations from the FL framework were observed only in specific cases, such as one-dimensional Luttinger liquids [15], small Fermi surfaces [16], systems with flat bands [17,18], and strongly correlated materials near quantum critical points. The tomographic regime represents a significant departure from these established scenarios, with profound implications for the understanding of hydrodynamic electron transport and electrodynamic response in low-dimensional materials.

Despite its fundamental importance, experimental verification of the tomographic Fermi liquid (TFL) hypothesis remains a significant challenge. The only known approach involves measuring electron viscosity as a function of various tuning parameters—including sample width W [10], frequency ω [19], and temperature T [20]—and comparing the observed functional dependencies with predictions from both conventional and tomographic Fermi liquid theories. However, electron viscosimetry [21] itself presents substantial technical difficulties due to unavoidable residual

*Contact author: dab@nus.edu.sg
†Contact author: svintcov.da@mipt.ru

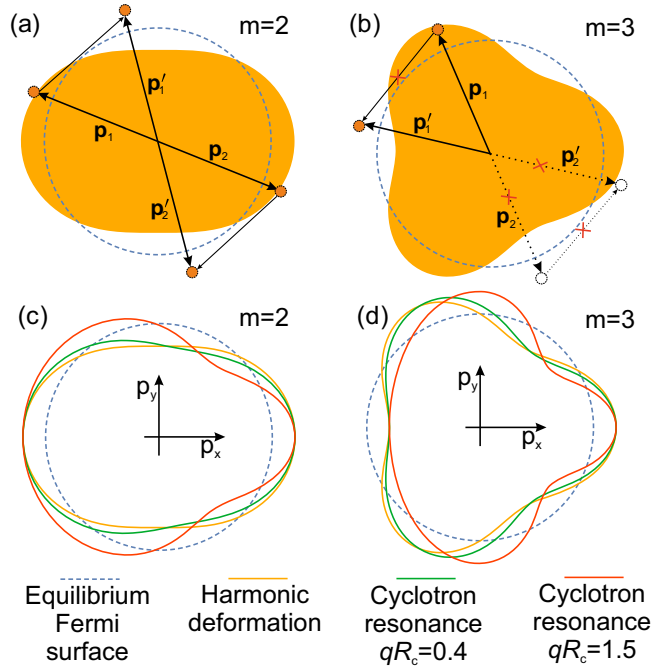

FIG. 1. Electron collisions in two dimensions and cyclotron resonance. Head-on electron-electron collisions, shown in (a) and (b), result in strong momentum relaxation of high-order ($m \geq 2$) harmonic deformations of the Fermi sphere. However, such collisions are impossible for odd harmonics [$m = 3$ is shown in (b) as an example], where an electron (orange dot) does not have a "partner" for collision (empty dot) on the opposite end of the deformed Fermi surface. (c) and (d) show the similarity between harmonic Fermi surface deformations (orange line) and its deformations under high-order cyclotron resonances (red and green lines). The green line corresponds to an almost uniform field ($qR_c = 0.4$) and the red line to a nonuniform field with $qR_c = 1.5$.

scattering from impurities and phonons. Furthermore, the similar scaling exponents predicted by conventional FL and TFL theories for viscosity make it challenging to definitively distinguish between these regimes experimentally.

In this Letter, we show that high-order cyclotron resonance (CR) [22–25] provides unique insights into the relaxation times of angular harmonics of the distribution function. Upon high-order resonance, an electron absorbs radiation with frequency ω of several cyclotron frequencies $m\omega_c$, $m \geq 2$, $\omega_c = e|B|/m^*$, B is the magnetic field, and m^* is the effective mass. The high-order CR emerges in nonuniform electromagnetic fields, which appear upon illumination of deep subwavelength structures. We prove that the width of the mth cyclotron resonance, Γ_m, and the relaxation rate of the mth distribution function harmonic, γ_m, are equal, i.e., $\gamma_m = \Gamma_m$. This relation holds under weak scattering conditions, $\gamma_m \ll \omega_c$, and for relatively uniform electromagnetic fields, $qR_c \ll 1$, where R_c is the cyclotron radius and q is the wave vector. In highly nonuniform fields with $qR_c \sim 1$, a more general relation between Γ_m and γ_m emerges. We further measure the widths of sequential CR peaks [26] in high-mobility doped graphene and find that even and odd distribution harmonics relax at different rates, providing direct experimental support for the TFL hypothesis.

The relation between mth-order CR linewidth and relaxation rate of mth angular harmonic can be understood as follows. The electromagnetic field changes its direction m times during the mth-order cyclotron resonance, causing an m-fold deformation of the Fermi surface, $\delta f(\theta_p) \propto e^{im\theta_p}$; see Figs. 1(c) and 1(d). The field nonuniformity adds a phase factor $e^{iqR_c \sin\theta_p}$ to the distribution function (see Refs. [27,28] and Supplemental Material Sec. I [29]). Still, this phase factor makes no effect on linewidth in the limit $qR_c \ll 1$.

We proceed to a rigorous solution of the CR problem in tomographic Fermi liquid. For this purpose, we solve the kinetic equation for an ac field-induced correction δf to the distribution function:

$$-i\omega\delta f + iqv_F \cos\theta_p \delta f - e\frac{\partial f_0}{\partial \mathbf{p}}\mathbf{E} + \omega_c \frac{\partial \delta f}{\partial \theta} = \mathcal{C}_{ee}\{\delta f\}. \quad (1)$$

Above, $\mathbf{q}$ is the wave vector directed along the x axis, $\mathbf{E} \propto \exp(-i\omega t + i\mathbf{qr})$ is the small ac electric field causing the CR directed, v_F is the Fermi velocity in a two-dimensional electron system (2DES), θ is the angle between electron momentum and direction of field nonuniformity $\mathbf{q}$, and $\mathcal{C}_{ee}$ is the electron-electron collision integral. We further introduce the parametrization of distribution function in terms of angular harmonics:

$$\delta f = \frac{\partial f_0}{\partial \varepsilon}\sum_m \chi_m e^{im\theta_p}. \quad (2)$$

The harmonic coefficients χ_m with the dimension of energy now weakly depend on ε, and the principal energy dependence is absorbed in the prefactor $\partial f_0/\partial\varepsilon$. The main convenience of representation (2) is the simple structure of collision integral in the harmonics' basis, guaranteed by the rotational invariance:

$$\mathcal{C}_{ee}\{\chi_m\} = -\gamma_m \chi_m. \quad (3)$$

Above, we have introduced the relaxation rates for mth angular harmonics of the distribution function $\gamma_m = 1/\tau_m$. The lowest three rates are zeros due to conservation of particle number and momentum upon collisions, $\gamma_{0,\pm1} = 0$ [38]. According to the tomographic Fermi liquid hypothesis, further harmonics satisfy $\gamma_{\text{even}} \gg \gamma_{\text{odd}}$. In further numerical calculations, we shall take all even and all

odd relaxation rates as identical $\gamma_{2k} \equiv \gamma_{\text{even}}$, $\gamma_{2k+1} \equiv \gamma_{\text{even}}$, $k = 1, 2, 3\ldots$. Our symbolic results remain applicable to arbitrary dependences of γ_m on harmonic number m.

Further on, it would be convenient to present the kinetic equation in the operator form similar to that used in quantum mechanics [10,12]. We introduce the ket vector for the distribution function $|\chi\rangle$ related to the angular harmonics $|m\rangle$ as $|\chi\rangle = \sum \chi_m |m\rangle$ and the ket vector for the electric forces $|F\rangle$ as

$$|F\rangle = i\frac{ev_F}{\sqrt{2}}(E_+|1\rangle + E_-|-1\rangle). \tag{4}$$

Above, $E_\pm = (E_x \pm iE_y)/\sqrt{2}$ are the amplitudes of circularly polarized electric fields. With these notations, the kinetic equation becomes

$$(\omega\hat{I} - \hat{H} + i\hat{C}_{ee})|\chi\rangle = |F\rangle. \tag{5}$$

Here, $\hat{I}$ is the identity operator, the "dynamic matrix" $\hat{H}$ governs the classical electron motion in the magnetic field and has the tridiagonal structure:

$$\hat{H} = \begin{pmatrix} \cdots & \cdots & 0 & 0 & 0 \\ qv_F/2 & (m+1)\omega_c & qv_F/2 & 0 & 0 \\ 0 & qv_F/2 & m\omega_c & qv_F/2 & 0 \\ 0 & 0 & qv_F/2 & (m-1)\omega_c & qv_F/2 \\ 0 & 0 & 0 & \cdots & \cdots \end{pmatrix}, \tag{6}$$

and $\hat{C}_{ee} = \text{diag}\{\gamma_m\}$ is the matrix representation of the e-e collision integral.

The solution of (5) is reached once the eigenfrequencies $\omega_s + i\Gamma_s$ and eigenvectors $|s\rangle$ of the dynamic operator $\hat{H} - i\hat{C}_{ee}$ are found. The former correspond to the frequencies and linewidths of the sth-order cyclotron resonances. Performing the operator inversion, we find the distribution function $|\chi\rangle$ and the conductivity tensor

$$\sigma_{\alpha\beta} = \sigma_D \sum_{s=-\infty}^{+\infty} \frac{\omega}{\omega - \omega_s - i\Gamma_s}\langle s|\alpha\rangle\langle\beta|s\rangle, \tag{7}$$

where $\sigma_D = ie^2v_F^2\rho(\varepsilon_F)/2\omega$ is the high-frequency Drude conductivity and $\rho(\varepsilon_F)$ is the density of states at the Fermi level. Equation (7) is applicable both to the 2D electron systems with parabolic bands (e.g., GaAs-based quantum wells) and to the massless electrons in graphene. It also applies in both the circular and Cartesian bases. In the first case, α and β take on the values of $+1$ for the right-circular field and -1 for the left-circular field. In the second case, $\alpha = \{x, y\}$ and $\beta = \{x, y\}$ enumerate the Cartesian axes. The Cartesian eigenvectors are related to the angular harmonics via $|x\rangle = (|+\rangle + |-\rangle)/\sqrt{2}$ and $|y\rangle = (|+\rangle - |-\rangle)/\sqrt{2}i$.

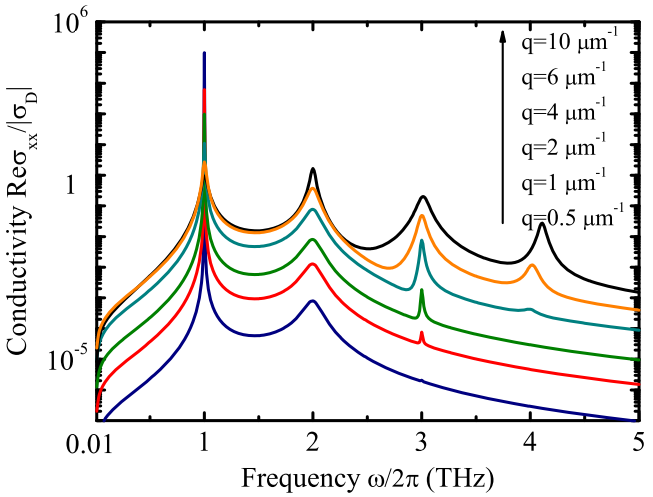

FIG. 2. The real part of the longitudinal 2DES conductivity $\text{Re}\sigma_{xx}$, normalized by the collisionless Drude conductivity $\sigma_D = [(ne^2)/(m\omega)]$ for different values of q with $\tau_{\text{even}} = 2$ ps, $\gamma_{\text{odd}} = 10$ ps, and $\omega_c/2\pi = 1$ THz.

The calculated frequency-dependent conductivity of the tomographic Fermi liquid (7) is shown in Fig. 2 [39]. The real part of the conductivity displays sharp resonances at $\omega = m\omega_c, m \geq 1$. The cyclotron harmonics become stronger with increasing the field nonuniformity, i.e., at larger q. The main CR broadens at larger q, which is a consequence of the viscous character of damping in FL. So far, all these observations are in agreement with previous studies of CR in 2DES with weak carrier-carrier collisions [28,40,41].

A distinctive feature of tomographic electron fluid is the relation between widths of subsequent cyclotron resonances. Namely, the third CR in Fig. 2 is very narrow compared to the second one, while the fourth is broad again. This alternating character of the resonance widths is a direct consequence of slow decay of the odd distribution harmonics and fast decay of even ones. The above rule holds as soon as the field remains uniform, $qR_c \ll 1$. For a cyclotron frequency $\omega_c/2\pi = 1$ THz and Fermi velocity $v_F = 10^6$ m/s, the cyclotron radius is estimated as $R_c \approx 0.15$ μm. In highly nonuniform fields (black curve in Fig. 2), seemingly all harmonics are equally broad, though the situation is even more intricate.

As apparent from conductivity spectra, the width of CR is the quantity affected by the tomographic nature of the 2D Fermi liquid. A direct measure of this width is the imaginary part of eigenfrequency Γ_s. To access it analytically, we apply the perturbation theory for the operator $\hat{H} - i\hat{C}_{ee}$, considering the collisions as a small perturbation. From a mathematical viewpoint, $\hat{H}$ is equivalent to the Hamiltonian of the tight-binding chain in a dc electric field, ω_c playing the role of voltage drop along one cell, and $qv_F/2$ playing the

role of hopping integral. The eigenvalues of $\hat{H}$ are perfectly localized each at sth harmonic (atomic site) in the absence of spatial dispersion (hopping). This implies the identity between cyclotron resonances $|s\rangle$ and angular harmonics $|m\rangle$ in the limit $qR_c \ll 1$. In this limit, inclusion of collisions trivially adds the damping $\Gamma_s = \gamma_s$ to each eigenfrequency.

In the presence of spatial dispersion, the eigenvectors of $\hat{H}$ are spread across various angular harmonics (atomic sites) according to [42]

$$\langle m|s\rangle = J_{|s-m|}(qR_c), \tag{8}$$

where $J_l(x)$ is the Bessel function of the lth order. The first-order perturbative correction to the frequency of the spatially dispersive states (8) is purely imaginary and given by

$$\delta\omega = \langle s|i\hat{C}_{ee}|s\rangle = i\Gamma_s, \tag{9}$$

$$\Gamma_s = J_0(qR_c)^2\gamma_s + \sum_{i=1}^{\infty} J_i(qR_c)^2(\gamma_{s+i} + \gamma_{s-i}). \tag{10}$$

Figure 3 illustrates the main features of cyclotron linewidth. In Fig. 3(a), we prove that variations of the odd angular harmonic lifetimes γ_{odd} affect only the width of odd-s cyclotron resonances in weakly nonuniform fields $qR_c \ll 1$. One observes that all odd and all even Γ_s coalesce onto two curves. The linewidths Γ_{2k} are not affected by variations of γ_{odd} at all. Figure 3(b) displays the wave vector dependences of linewidths. The odd linewidths, being initially small, start growing at $qR_c \sim 1$. This occurs due to the "admixture" of the even angular harmonics to the odd cyclotron resonance. Remarkably, the linewidths of the even CRs (say, second and fourth) can drop down to the very small values. This occurs due to the oscillatory nature of the spectral weight $|J_0(qR_c)|^2$ and happens at qR_c equal to the zeros of Bessel function J_0. We finally note that the general expression for the linewidth (9) reproduces the viscous damping of the principal CR $\Gamma_1 \propto q^2$ at small wave vectors [28,40,41].

The experimental test of the TFL hypothesis now amounts to the measurement of the 2D conductivity at a given wave vector and frequency $\sigma(q,\omega)$. Its real part governs the absorbed power $P_{\text{abs}} = 1/2\sum_q \sigma'(q,\omega)|E_{q\omega}|^2$, where $E_{q\omega}$ is the spectral composition of the electric ac field in the 2DES plane. One method for measuring P_{abs} relies on transmission spectroscopy of grating-gated 2DES [25]. Such data are available only for the 2DES with modulated lateral doping [22,23], which complicates their analysis.

Another powerful technique for measuring the absorption spectra of low-dimensional systems relies on the photoresistance [43–45], i.e., the change in the dc resistance ΔR_{xx} induced by radiation. It relies on the fact that ΔR_{xx} is proportional to the absorbed electromagnetic power, and resonances in absorption at certain ω and B should greatly enhance the measured value of ΔR_{xx}.

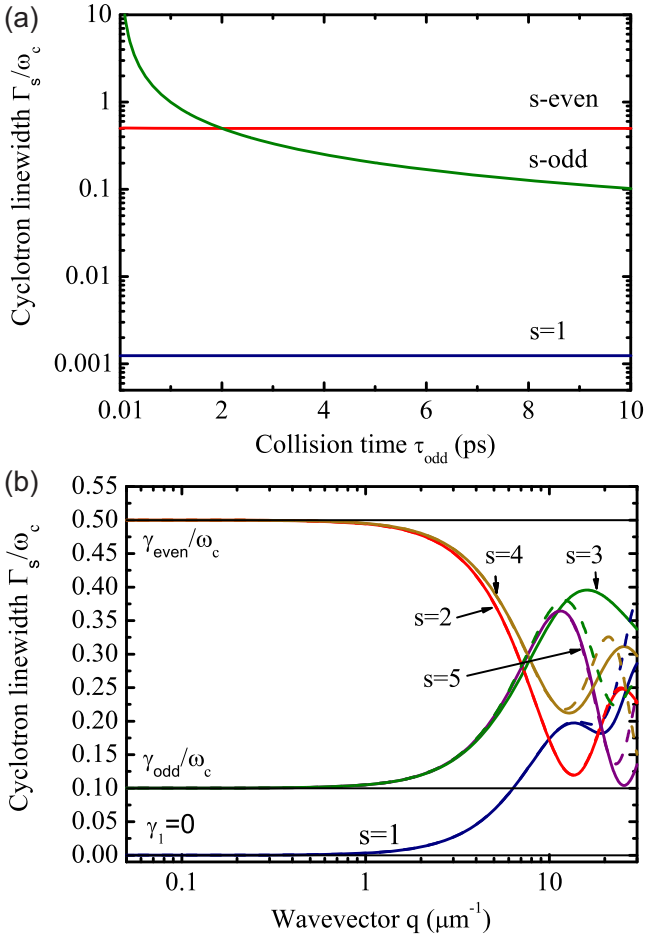

FIG. 3. Cyclotron linewidths Γ_s in the tomographic Fermi liquid. (a) Γ_s in units of ω_c vs variable relaxation time of odd angular harmonics γ_{odd} with constant $\tau_{\text{even}} = 2$ ps. Wave vector $q = 1$ μm^{-1}. (b) Linewidth Γ_s for several lowest $s = 1\ldots5$ vs wave vector of the electromagnetic field q. The results obtained by numerical diagonalization of dynamic matrix are shown with solid lines; the analytical result of the perturbation theory is shown by the dashed ones. In both panels, charge carrier concentration is $n = 10^{12}$ cm^{-2} and cyclotron frequency $\omega_c/2\pi = 1$ THz.

We have performed the photoresistance measurements on a high-quality graphene sample in classically strong magnetic fields $B < 1$ T. The CR and its harmonics were excited by coherent THz radiation generated by a continuous wave optically pumped molecular laser. Details on sample fabrication and experimental technique can be found in Supplemental Secs. II and III [29]. We intentionally fabricated narrow (∼1 μm in width) metallic Hall contacts to the sample partially embedding into the channel. This configuration provides highly nonuniform electromagnetic fields and is, thus, particularly suitable for observation of high-order CRs [46].

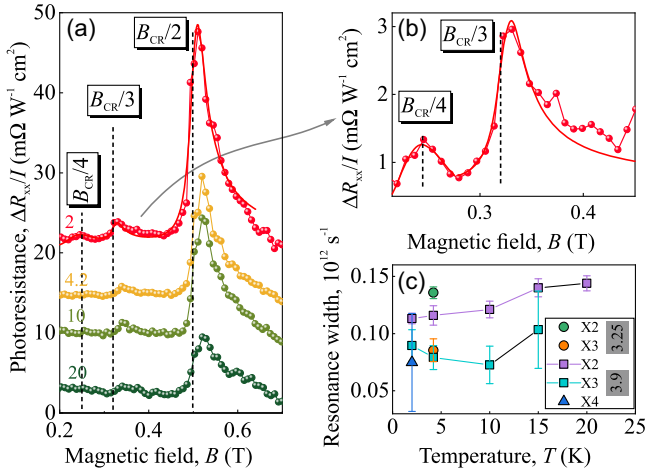

FIG. 4. Measured graphene photoresistance (PR) as a function of the magnetic field for different values of temperature. The PR is defined as a change in a longitudinal resistance upon illumination ΔR_{xx}, normalized by radiation intensity I. (a) shows the B-dependent PR in the vicinity of second, third, and fourth CR harmonics at different temperatures (marked by numbers); (b) shows the magnified view of PR at $T = 2$ K in the vicinity of third and fourth harmonics. Solid lines show the fit according to Eq. (11); dashed vertical lines label the theoretically anticipated position of the CR. Radiation frequency is $f = 0.69$ THz; carrier density is 3.9×10^{12} cm^{-2}. (c) Extracted widths of the second (X2) and third (X3) cyclotron resonances at different temperatures. Green and orange data points were obtained at a different carrier density $n_s = 3.25 \times 10^{12}$ cm^{-2} and $T = 4$ K (raw data in Supplemental Sec. IV [29]).

Figures 4(a) and 4(b) show the example of the measured photoresistance at $f = 0.69$ THz and $n_s = 3.9 \times 10^{12}$ cm^{-2}, where up to three CR overtones ($s = 2 \ldots 4$) are observed. We note that the PR signal at the main $s = 1$ CR is very weak at that frequency and density but reappears at larger f and n_s (Supplemental Sec. IV [29]) [47]. At given n_s controlled by the back gate, we confidently identify all spikes to CR or its harmonics according to $B = 2\pi m f/|e|s$, where s is an integer and $m = \hbar\sqrt{\pi n_s}/v_F$ for single-layer graphene. The anticipated resonance positions are marked by vertical dashed lines in Figs. 4(a) and 4(b) and agree well with observed photoresistance peaks. This agreement enables further linewidth analysis.

To reproduce the highly asymmetric shape of the absorption, one has to account for the plasmonic effects, i.e., screening of the incident field E_0 by the 2D electrons [25,48]. They are taken into account by relating the total field $E_{q\omega}$ to the incident field E_0 via the dielectric function of 2DES $\epsilon(q,\omega)$, $E_{q\omega} = E_0/\epsilon(q,\omega)$. The dominant contribution to the antiscreening comes from the waves with nearly zero group velocity, the so-called Bernstein modes [49–51]. In such a situation, the spectral dependence of absorbed power is suitably described by [26]

$$P_{\rm abs}(\omega_c) = P_0 + \sum_{s=2}^{\infty} A_s \mathrm{Re}\left(\frac{1}{\sqrt{\omega_s^* - \omega_c + i\Gamma_s}}\right). \quad (11)$$

Expression (11) is different from a more common Lorentzian fit due to the continuous spectrum of 2D plasmons in the vicinity of each cyclotron harmonic. Its functional form does not depend on the composition of substrates, yet the coefficients P_0 and A_s do; see Supplemental Sec. V for a derivation [29].

We extracted the linewidths Γ_s of cyclotron resonances by fitting the photoresistance data with model (11) considering A_s, ω_s^*, and Γ_s as fitting parameters. The extracted values of Γ_s together with their error bars are shown in Fig. 4(c). The fitting procedure shows that third-order CR is systematically narrower than the second-order one at all temperatures where it is seen, $2\ \mathrm{K} < T < 20\ \mathrm{K}$ [52]. This fact agrees with TFL hypothesis qualitatively. Namely, relaxation of the odd-order (third) cyclotron resonance appears to be weaker than that of the even order (second). The theory outlined above traces this fact to the different relaxation rates of even- and odd-order distribution functions.

The small scattering rate of the third harmonic of distribution function, as compared to the second one, cannot be explained within impurity or electron-phonon scattering models. It is easy to show that both models predict stronger relaxation with increasing the harmonic number m (see Ref. [53] and Supplemental Sec. VI [29]). The TFL hypothesis is currently the only one capable of explaining the unusual relation $\Gamma_3 < \Gamma_2$. Still, it is worth noting that the impurity scattering contributes to the observed linewidth by providing finite $\Gamma_s(T \to 0)$. The *excess* linewidth $\Gamma_2(T = 20\ \mathrm{K}) - \Gamma_2(T = 4\ \mathrm{K}) \approx 3 \times 10^{10}\ \mathrm{s}^{-1}$ agrees, by the order of magnitude, with normal Coulomb scattering lifetime in 2DES given by [54] $\pi/(8\hbar)(kT)^2/\varepsilon_F = 4 \times 10^{10}\ \mathrm{s}^{-1}$ for $\varepsilon_F = 100$ meV. At the same time, Γ_3 shows no systematic temperature dependence within the accuracy of experiment. This is not unusual, as $\gamma_{\rm odd}$ for e-e collisions should be, in theory, by a factor of T^2/ε_F^2 smaller than $\gamma_{\rm even}$ and undetectable even in the cleanest samples. A smaller contribution of impurities to the observed CR linewidth is anticipated in high-mobility GaAs quantum wells [55,56] and ultracold atomic Fermi gases [7,8].

In conclusion, we have shown that the width of mth-order cyclotron resonance in a two-dimensional system is linked to the relaxation rate of the mth angular harmonic of the distribution function. For long-wavelength fields, these two quantities are exactly equal. The magnetoabsorption data of high-quality graphene at THz frequencies point out the weaker relaxation of the third-order CR, as compared to the second-order one. Such an anomalous relation between relaxation rates of the second and third angular harmonics of distribution function points to the validity of tomographic Fermi liquid hypothesis.

Acknowledgments—The work of I. M., K. K., and D. S. was supported by the Ministry of Science and Higher Education of the Russian Federation (Grant No. FSMG-2025-0005). S. G. and E. M. acknowledge the financial support of the Deutsche Forschungsgemeinschaft (DFG, German Research Foundation) via Project-ID No. 314695032—SFB 1277 (Subproject A04) and of the Volkswagen Stiftung Program (97738). D. A. B. acknowledges the support from Singapore Ministry of Education AcRF Tier 2 grant T2EP50123-0020 and AcRF Tier 1 grant 22-5390-P0001.

[1] A. Lucas and K. C. Fong, Hydrodynamics of electrons in graphene, J. Phys. Condens. Matter **30**, 053001 (2018).
[2] M. J. M. de Jong and L. W. Molenkamp, Hydrodynamic electron flow in high-mobility wires, Phys. Rev. B **51**, 13389 (1995).
[3] A. Aharon-Steinberg, T. Völkl, A. Kaplan, A. K. Pariari, I. Roy, T. Holder, Y. Wolf, A. Y. Meltzer, Y. Myasoedov, M. E. Huber, B. Yan, G. Falkovich, L. S. Levitov, M. Hücker, and E. Zeldov, Direct observation of vortices in an electron fluid, Nature (London) **607**, 74 (2022).
[4] G. Varnavides, A. Yacoby, C. Felser, and P. Narang, Charge transport and hydrodynamics in materials, Nat. Rev. Mater. **8**, 726 (2023).
[5] E. Shuryak, Why does the quark–gluon plasma at RHIC behave as a nearly ideal fluid?, Prog. Part. Nucl. Phys. **53**, 273 (2004), heavy Ion Reaction from Nuclear to Quark Matter.
[6] R. A. Davison, K. Schalm, and J. Zaanen, Holographic duality and the resistivity of strange metals, Phys. Rev. B **89**, 245116 (2014).
[7] C. Cao, E. Elliott, J. Joseph, H. Wu, J. Petricka, T. Schäfer, and J. E. Thomas, Universal quantum viscosity in a unitary Fermi gas, Science **331**, 58 (2011).
[8] J. Maki, U. Gran, and J. Hofmann, Odd-parity effect and scale-dependent viscosity in atomic quantum gases, arXiv:2408.02738.
[9] R. N. Gurzhi, A. N. Kalinenko, and A. I. Kopeliovich, Electron-electron collisions and a new hydrodynamic effect in two-dimensional electron gas, Phys. Rev. Lett. **74**, 3872 (1995).
[10] P. Ledwith, H. Guo, A. Shytov, and L. Levitov, Tomographic dynamics and scale-dependent viscosity in 2D electron systems, Phys. Rev. Lett. **123**, 116601 (2019).
[11] H. Buhmann and L. Molenkamp, 1D diffusion: A novel transport regime in narrow 2DEG channels, Physica (Amsterdam) **12E**, 715 (2002).
[12] P. J. Ledwith, H. Guo, and L. Levitov, The hierarchy of excitation lifetimes in two-dimensional Fermi gases, Ann. Phys. (Amsterdam) **411**, 167913 (2019).
[13] R. N. Gurzhi, A. N. Kalinenko, and A. I. Kopeliovich, Electron-electron momentum relaxation in a two-dimensional electron gas, Phys. Rev. B **52**, 4744 (1995).
[14] J. Hofmann and U. Gran, Anomalously long lifetimes in two-dimensional Fermi liquids, Phys. Rev. B **108**, L121401 (2023).
[15] H. Ishii, H. Kataura, H. Shiozawa, H. Yoshioka, H. Otsubo, Y. Takayama, T. Miyahara, S. Suzuki, Y. Achiba, M. Nakatake, T. Narimura, M. Higashiguchi, K. Shimada, H. Namatame, and M. Taniguchi, Direct observation of Tomonaga–Luttinger-liquid state in carbon nanotubes at low temperatures, Nature (London) **426**, 540 (2003).
[16] A. A. Abrikosov and S. D. Beneslavskii, Possible existence of substances intermediate between metals and dielectrics, Sov. Phys. JETP **32**, 699 (1971), http://jetp.ras.ru/cgi-bin/dn/e_032_04_0699.pdf.
[17] P. Kumar, S. Peotta, Y. Takasu, Y. Takahashi, and P. Törmä, Flat-band-induced non-Fermi-liquid behavior of multicomponent fermions, Phys. Rev. A **103**, L031301 (2021).
[18] S. Sayyad, E. W. Huang, M. Kitatani, M.-S. Vaezi, Z. Nussinov, A. Vaezi, and H. Aoki, Pairing and non-Fermi liquid behavior in partially flat-band systems: Beyond nesting physics, Phys. Rev. B **101**, 014501 (2020).
[19] J. Hofmann and S. Das Sarma, Collective modes in interacting two-dimensional tomographic Fermi liquids, Phys. Rev. B **106**, 205412 (2022).
[20] S. Kryhin, Q. Hong, and L. Levitov, Linear-in-temperature conductance in two-dimensional electron fluids, Phys. Rev. B **111**, L081403 (2025).
[21] R. Krishna Kumar, D. A. Bandurin, F. M. D. Pellegrino, Y. Cao, A. Principi, H. Guo, G. H. Auton, M. Ben Shalom, L. A. Ponomarenko, G. Falkovich, K. Watanabe, T. Taniguchi, I. V. Grigorieva, L. S. Levitov, M. Polini, and A. K. Geim, Superballistic flow of viscous electron fluid through graphene constrictions, Nat. Phys. **13**, 1182 (2017).
[22] E. G. Mohr and D. Heitmann, Interaction of magnetoplasmons and cyclotron resonance harmonics in electron inversion layers on Si(100), J. Phys. C **15**, L753 (1982).
[23] J. Lefebvre, J. Beerens, Y. Feng, Z. Wasilewski, J. Beauvais, and E. Lavallée, Bernstein modes in a laterally modulated two-dimensional electron gas, Semicond. Sci. Technol. **13**, 169 (1998).
[24] D. E. Bangert, R. J. Stuart, H. P. Hughes, D. A. Ritchie, and J. Frost, Bernstein modes in grating-coupled 2DEGs, Semicond. Sci. Technol. **11**, 352 (1996).
[25] A. V. Chaplik and D. Heitmann, Geometric resonances of two-dimensional magnetoplasmons, J. Phys. C **18**, 3357 (1985).
[26] D. A. Bandurin, E. Mönch, K. Kapralov, I. Y. Phinney, K. Lindner, S. Liu, J. H. Edgar, I. A. Dmitriev, P. Jarillo-Herrero, D. Svintsov, and S. D. Ganichev, Cyclotron resonance overtones and near-field magnetoabsorption via terahertz Bernstein modes in graphene, Nat. Phys. **18**, 462 (2022).
[27] L. P. Pitaevskii and E. Lifshitz, *Physical Kinetics: Volume 10* (Butterworth-Heinemann, London, 2012), Vol. 10, Chap. 53. Distribution function in the magnetic field.
[28] K. Kapralov and D. Svintsov, Ballistic-to-hydrodynamic transition and collective modes for two-dimensional electron systems in magnetic field, Phys. Rev. B **106**, 115415 (2022).
[29] See Supplemental Material at http://link.aps.org/supplemental/10.1103/zq1g-8d4s for (I) the solution of CR problem in the collisionless system of 2D electrons, (II) details of sample fabrication, (III) experimental details

on THz photoresistance measurement, (IV) additional experimental data on photoresistance, (V) derivation of the absorption line shape, and (VI) theory of relaxation rates γ_m for impurity and phonon scattering, which includes Refs. [30–37].

[30] D. G. Purdie, N. M. Pugno, T. Taniguchi, K. Watanabe, A. C. Ferrari, and A. Lombardo, Cleaning interfaces in layered materials heterostructures, Nat. Commun. **9**, 5387 (2018).

[31] K. S. Novoselov, A. K. Geim, S. V. Morozov, D. Jiang, Y. Zhang, S. V. Dubonos, I. V. Grigorieva, and A. A. Firsov, Electric field in atomically thin carbon films, Science **306**, 666 (2004).

[32] S. D. Ganichev and W. Prettl, *Intense Terahertz Excitation of Semiconductors* (Oxford University Press, Oxford, 2005).

[33] N. N. Mikhailov, S. A. Dvoretskii, and J. C. Portal, Cyclotron resonance in a two-dimensional semimetal based on a HgTe quantum well, JETP Lett. **93**, 170 (2011).

[34] M. Otteneder, I. A. Dmitriev, S. Candussio, M. L. Savchenko, D. A. Kozlov, V. V. Bel'kov, Z. D. Kvon, N. N. Mikhailov, S. A. Dvoretsky, and S. D. Ganichev, Sign-alternating photoconductivity and magnetoresistance oscillations induced by terahertz radiation in HgTe quantum wells, Phys. Rev. B **98**, 245304 (2018).

[35] S. Hubmann, G. Di Battista, I. A. Dmitriev, K. Watanabe, T. Taniguchi, D. K. Efetov, and S. D. Ganichev, Infrared photoresistance as a sensitive probe of electronic transport in twisted bilayer graphene, 2D Mater. **10**, 015005 (2023).

[36] E. H. Hwang, S. Adam, and S. D. Sarma, Carrier transport in two-dimensional graphene layers, Phys. Rev. Lett. **98**, 186806 (2007).

[37] F. T. Vasko and V. Ryzhii, Voltage and temperature dependencies of conductivity in gated graphene, Phys. Rev. B **76**, 233404 (2007).

[38] A. A. Abrikosov and I. M. Khalatnikov, The theory of a Fermi liquid (the properties of liquid 3He at low temperatures), Rep. Prog. Phys. **22**, 329 (1959).

[39] Application of Eq. (7) requires the knowledge of eigenvectors $|s\rangle$ and eigenvalues $\omega_s + i\Gamma_s$ for the dynamic matrix. For arbitrary scattering strength, they can be found numerically by retaining a large (but finite) number of angular harmonics $m_{\max}$. The computational complexity here scales linearly with $m_{\max}$ due to the tridiagonal structure of the matrix. In the weak-scattering limit, the perturbative results (8) and (9) apply.

[40] F. M. D. Pellegrino, I. Torre, and M. Polini, Nonlocal transport and the Hall viscosity of two-dimensional hydrodynamic electron liquids, Phys. Rev. B **96**, 195401 (2017).

[41] P. S. Alekseev, Magnetic resonance in a high-frequency flow of a two-dimensional viscous electron fluid, Phys. Rev. B **98**, 165440 (2018).

[42] M. Saitoh, Electronic states in a finite linear crystal in an electric field, J. Phys. C **6**, 3255 (1973).

[43] E. Vasiliadou, G. Müller, D. Heitmann, D. Weiss, K. V. Klitzing, H. Nickel, W. Schlapp, and R. Lösch, Collective response in the microwave photoconductivity of Hall bar structures, Phys. Rev. B **48**, 17145 (1993).

[44] I. V. Kukushkin, V. M. Muravev, J. H. Smet, M. Hauser, W. Dietsche, and K. von Klitzing, Collective excitations in two-dimensional electron stripes: Transport and optical detection of resonant microwave absorption, Phys. Rev. B **73**, 113310 (2006).

[45] Z.-D. Kvon, S. N. Danilov, N. N. Mikhailov, S. A. Dvoretsky, W. Prettl, and S. D. Ganichev, Cyclotron resonance photoconductivity of a two-dimensional electron gas in HgTe quantum wells, Physica (Amsterdam) **40E**, 1885 (2008).

[46] P. Alonso-Gonzalez, A. Y. Nikitin, F. Golmar, A. Centeno, A. Pesquera, S. Velez, J. Chen, G. Navickaite, F. Koppens, A. Zurutuza, F. Casanova, L. E. Hueso, and R. Hillenbrand, Controlling graphene plasmons with resonant metal antennas and spatial conductivity patterns, Science **344**, 1369 (2014).

[47] A possible reason for CR weakening at large n_s lies in radiative damping [48], i.e., screening of the incident radiation by highly conductive 2DES.

[48] V. M. Muravev, I. V. Andreev, S. I. Gubarev, V. N. Belyanin, and I. V. Kukushkin, Fine structure of cyclotron resonance in a two-dimensional electron system, Phys. Rev. B **93**, 041110(R) (2016).

[49] Y. Dai, R. R. Du, L. N. Pfeiffer, and K. W. West, Observation of a cyclotron harmonic spike in microwave-induced resistances in ultraclean GaAs/AlGaAs quantum wells, Phys. Rev. Lett. **105**, 246802 (2010).

[50] S. I. Dorozhkin, A. A. Kapustin, V. Umansky, and J. H. Smet, Absorption of microwave radiation by two-dimensional electron systems associated with the excitation of dimensional Bernstein mode resonances, JETP Lett. **113**, 670 (2021).

[51] V. A. Volkov and A. A. Zabolotnykh, Bernstein modes and giant microwave response of a two-dimensional electron system, Phys. Rev. B **89**, 121410(R) (2014).

[52] Note that no saturation effects are observed, even at the highest power levels (see Fig. S5 in Supplemental Material), suggesting that the heating of the electron gas remains well controlled throughout the measurement.

[53] G. Baker, M. Moravec, and A. P. Mackenzie, A perspective on non-local electronic transport in metals: Viscous, ballistic, and beyond, Ann. Phys. (Berlin) **536**, 2400087 (2024).

[54] L. Zheng and S. D. Sarma, Coulomb scattering lifetime of a two-dimensional electron gas, Phys. Rev. B **53**, 9964 (1996).

[55] A. D. Levin, G. M. Gusev, A. S. Yaroshevich, Z. D. Kvon, and A. K. Bakarov, Geometric engineering of viscous magnetotransport in a two-dimensional electron system, Phys. Rev. B **108**, 115310 (2023).

[56] L. V. Ginzburg, C. Gold, M. P. Röösli, C. Reichl, M. Berl, W. Wegscheider, T. Ihn, and K. Ensslin, Superballistic electron flow through a point contact in a ga[al]as heterostructure, Phys. Rev. Res. **3**, 023033 (2021).